IEEE Photonics Journal
An IEEE Photonics Society Publication

Restorative Self-Image of Rough-Line Grids: Application to Coherent EUV Talbot Lithography

Volume 8, Number 3, June 2016

Hyun-su Kim
Wei Li
Mario C. Marconi
William S. Brocklesby
Larissa Juschkin

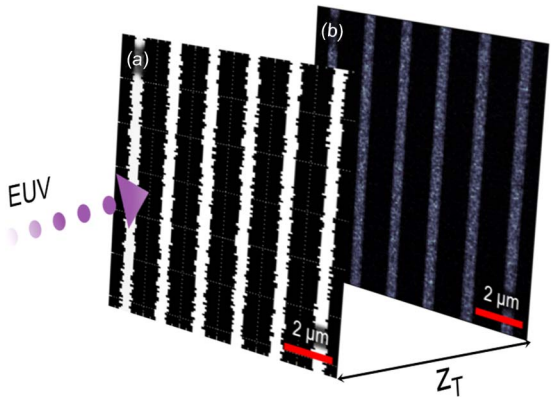

DOI: 10.1109/JPHOT.2016.2553847
1943-0655

IEEE photonics SOCIETY

IEEE

Restorative Self-Image of Rough-Line Grids: Application to Coherent EUV Talbot Lithography

Hyun-su Kim,[1,3,4] Wei Li,[2] Mario C. Marconi,[2] William S. Brocklesby,[3] and Larissa Juschkin[1,4]

[1]Chair for the Experimental Physics of EUV, RWTH Aachen University and Jülich Aachen Research Alliance, Fundamentals for Future Information Technology (JARA-FIT), 52074 Aachen, Germany
[2]Engineering Research Center for Extreme Ultraviolet Science and Technology and the Department of Electrical and Computer Engineering, Colorado State University, Fort Collins, CO 80523 USA
[3]Optoelectronics Research Centre, University of Southampton, Southampton SO17 1BJ, U.K.
[4]Peter Grünberg Institut (PGI-9), Forschungszentrum Jülich GmbH, Jülich Aachen Research Alliance, Fundamentals for Future Information Technology (JARA-FIT), 52425 Jülich, Germany

DOI: 10.1109/JPHOT.2016.2553847

Manuscript received March 26, 2016; accepted April 11, 2016. Date of publication April 13, 2016; date of current version April 28, 2016. The work of H. Kim was supported in part by the EU FP7 Erasmus Mundus Joint Doctorate Programme EXTATIC under framework partnership agreement FPA-2012-0033 and in part by the COST Action MP1203. The work of L. Juschkin was supported by the Helmholtz Association for a Helmholtz Professorship as a part of the Initiative and Networking Fund. The work of W. Li and M. Marconi was supported by the National Science Foundation through Award ECCS 1507907. Corresponding author: H. Kim (e-mail: lighttn@gmail.com).

Abstract: Self-imaging is a well-known optical phenomenon produced by diffraction of a coherent beam in a periodic structure. The self-imaging effect (or Talbot effect) replicates the field intensity at a periodic mask in certain planes, effectively producing in those planes an image of the mask. However, the effect has not been analyzed for a rough-line grid from the point of view of the fidelity of the image. In this paper, we investigate the restorative effect of the self-image applied to the lithography of gratings with rough lines. This paper is applied to characterize a Talbot lithography experiment implemented in the extreme ultraviolet. With the self-imaging technique, a mask with grid patterns having bumps randomly placed along the line edges reproduces a grid pattern with smoothed line edges. Simulation explores the approach further for the cases of sub-100-nm pitch grids.

Index Terms: Talbot effect, nanofabrication, Extreme ultraviolet application.

1. Introduction

In this work, we analyze the restoration effect produced in Talbot images applied to nanolithography. Talbot lithography in the extreme ultraviolet (EUV) has been demonstrated as a convenient method to fabricate nanostructures. The technique is of a great interest for many applications, requiring well-defined periodic structures, such as defect free solar cells, semiconductor photonic devices fabrication, or pre-patterning for self-assembled growth of quantum dots (QDs) arrays [1].

The Talbot effect, or self-imaging, is a well-known optical phenomenon. When a coherent plane wave impinges on a periodic object such as a grating, an image is generated at regular

distances away from the object. This distance, i.e., the so-called Talbot distance (z_T), is determined by

$$z_T = 2 \cdot d^2/\lambda \tag{1}$$

where d is the pitch (period) of the object structures, and λ is the wavelength of illumination [2], [3]. The Talbot pattern is repeated in the planes located at distances $z = n \cdot zT$, where n is a positive integer. The self-imaging effect can be utilized in lithography to replicate nanoscale periodic structures illuminating a periodic mask with coherent EUV radiation. This approach called EUV Talbot lithography has been examined in many aspects, e.g., showing its capability to replicate complex patterns [4], the possibility to obtain spatial frequency multiplication [5], and the characteristic of defect tolerant printing [6].

The quality of the patterned structures is important, because it influences the functionality of the device. The fidelity of the printed pattern is particularly critical in the fabrication of microelectronics components. The microelectronic industry had invested significant amount of effort and resources to mitigate this problem, localizing and repairing defects in the lithography masks. However, in addition, in other applications besides the main stream of the microcomponents industry, the quality of the lithography print is instrumental to a successful device fabrication and performance.

Talbot lithography is particularly well adapted to produce high quality lithography prints with high resolution over large areas. It has been shown that the Talbot effect can reproduce the defect free images from a defective periodic mask. This filtering characteristic was identified as a convenient way to improve the quality of the print in a lithography process [7], [8]. The defect tolerance characteristic of the Talbot images is well studied in the bibliography. It was shown that a mask with a periodic pattern, which is locally damaged, produces a defect-free copy at the Talbot distance. The effect of a defect on the pattern size around the defect in ArF Talbot lithography was investigated for submicron patterns [9]. In this case, the periodic mask included regularly distributed defects. On the other hand, it was shown how the presence of spherical particles behind gratings affects the formation of Talbot self-images [10]. The tolerance in angles of continuously self-imaging gratings was studied for nonparaxial illumination both numerically and experimentally [11]. The defect tolerant Talbot imaging was studied for lithography applications with a EUV laser in the case of masks with complex designs [6], [12]. For the particular case of a line grating, it is increasingly difficult to fabricate a straight-line edge when the pitch is reduced. Thus, it would be worth to analyze the restoration effect of the Talbot image in this case, quantifying the quality of the replicated pattern for the rough-line grid. In this work, we analyze with numerical simulations and experimental results the effectiveness of EUV Talbot lithography to improve the lithography print from rough line grid masks. For the test we used a binary transmission mask fabricated in an opaque membrane with slits opened through it and a coherent EUV high-photon flux laser. We observed improvement in the pattern recorded in the photoresist compared with the original pattern on the mask. We also performed a model calculation of the obtained image for sub-100 nm pitches and analyzed the limits of the improvement.

2. Simulated Demonstration

Fig. 1 illustrates the scheme of the self-imaging effect. When the mask [Fig. 1(a)] is illuminated by a plane wave, a replica of the mask's pattern is observed at the Talbot plane z_T [Fig. 1(b)]. For the simulation, a line grid pattern with rough edges was created. Bumps of ~100 nm radius were randomly distributed along the line edges. The size of the bumps along the edges of the slits that produce the roughness was selected to be bigger than the cut-off size defined as $\Delta x \approx \lambda/2\pi \approx 7.5$ nm for the wavelength at 46.9 nm. This selection validates the results of the scalar theory used in the simulations. The distribution was performed using the random function in MATLAB's built-in functions. The diffraction pattern was calculated using the Fresnel diffraction formalism, by the fast Fourier transform method [13]. The scalar diffraction method assumes the mask as the thin mask approximation (TMA). The simulation is performed in a finite grid of

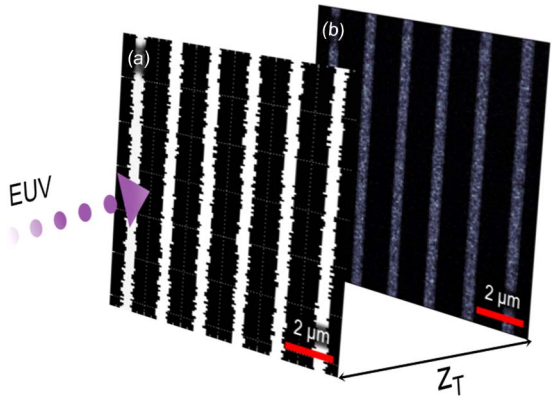

Fig. 1. Scheme of the self-imaging setup. (a) Talbot mask. (b) Self-image produced at a distance z_T.

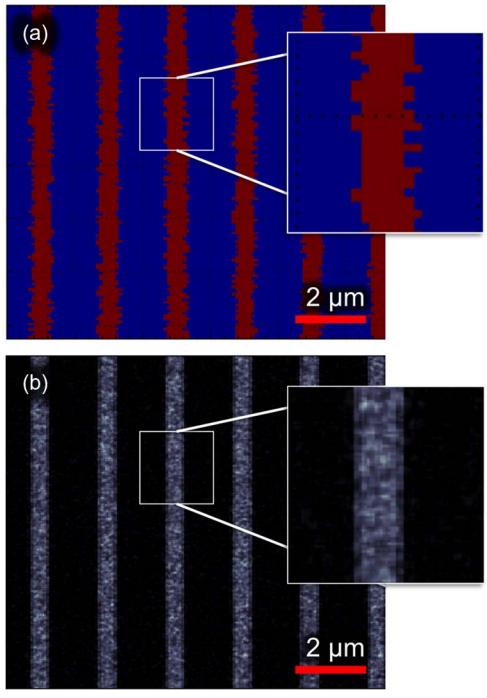

Fig. 2. Simulated images of (a) a mask with randomly rough lines and (b) the self-image at z_T.

$\Delta x = 0.5$ nm and $\Delta y = 0.5$ nm over a field of 50 μm $\times$ 50 μm in the mask. Fig. 2 shows the simulated images of (a) a mask with randomly rough lines and (b) the self-image at z_T.

The simulation shows that the self-image at z_T has significantly better quality, in which the bumps along edges are smoothed out over the grid. As a consequence the rough lines were straightened in the self-image. The roughness along an edge was quantified using standard deviation (σ) defined as

$$\sigma = \sqrt{\frac{1}{N} \cdot \sum_{i=1}^{N} (x_i - \overline{x})^2} \tag{2}$$

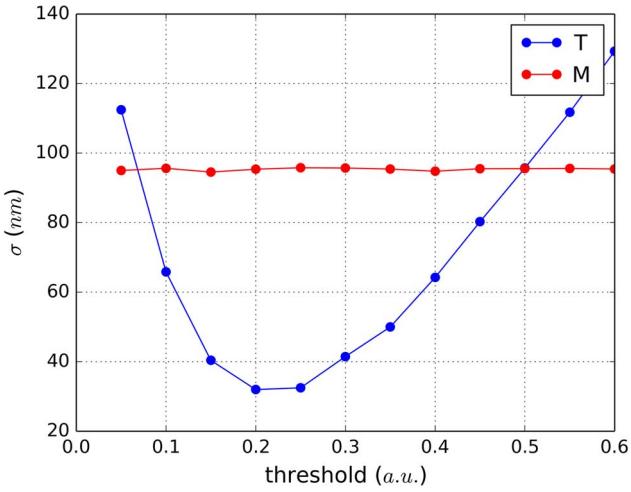

Fig. 3. The σ values on the self-image (T) in dependence of the threshold level and on the mask (M) in simulation.

where N is the number of samplings along a line, and the quantity in the bracket is the deviation of the edge of the slit from the straight line at the sampling point i. In the case of the self-image, the deviation of the edge is determined after a binary thresholding of the calculated image. Consequently the deviation of the edge depends on the value selected for the threshold. Fig. 3 shows the calculated σ for different threshold values ranging from 0.05 to 0.7. The calculated $\sigma = 95$ nm on the mask [see Fig. 2(a)] was reduced to $\sigma \cong 32$ nm in the Talbot pattern [Fig. 2(b)]. In the analysis, the parabolic curve of σ in the Talbot pattern occurred due to the irregular intensity distribution of the areal image of Talbot pattern. When the threshold value is either too high or low, the difference of intensity value between neighboring x_i can be very large. This causes the higher σ values in the areal image as compared with the value obtained for the mask.

3. Experimental Demonstration

The experimental demonstration was performed with an EUV laser and a transmission Talbot mask with a setup as following. The transmission mask and the wafer are aligned in the optical axis as illustrated in Fig. 1. The monochromatic EUV illumination of wavelength 46.9 nm was generated by a capillary discharge plasma laser [14]. The capillary discharge plasma produces a highly spatial and temporal coherent beam well suited for the application described in this work. The spatial coherence length at the position where the self image was obtained was around 350 μm, which covered the whole area of the mask, assuring a fully spatial coherent illumination. The temporal coherence of the laser is $\Delta\lambda/\lambda \approx 3.5 \times 10^{-5}$ [15]–[17]. The exposure dose at the sample plane was about 0.1–0.3 mJ/cm^2 per pulse [12], [18].

The transmission Talbot mask was defined using a focused ion beam (FIB) tool to drill through a low stressed Si_3N_4 membrane. The same binary file that was used for the simulation was fed into the FIB to make a more precise comparison between the calculation and the experimental results. After the milling, the mask was deposited with a layer of 50 nm of gold to improve the absorption in the EUV. The pitch in the mask was 2 μm, and the slit width was ~500 nm in average. The illumination field area of the mask was 50 μm $\times$ 50 μm. Fig. 4 shows the SEM image of the fabricated mask.

The depth of focus (DOF) in the Talbot plane is expressed as

$$\mathrm{DOF} = \frac{\lambda}{(\mathrm{NA})^2} = \lambda\left(1 + 4n^2\left(\frac{d^2}{\lambda \cdot A}\right)^2\right) \tag{3}$$

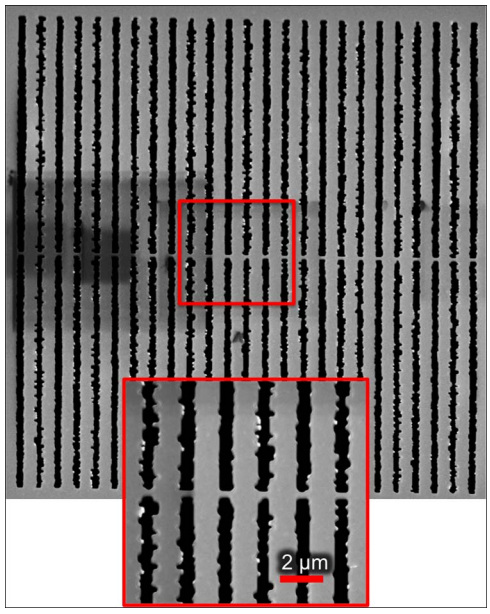

Fig. 4. Free-standing transmission mask having the rough lines grid.

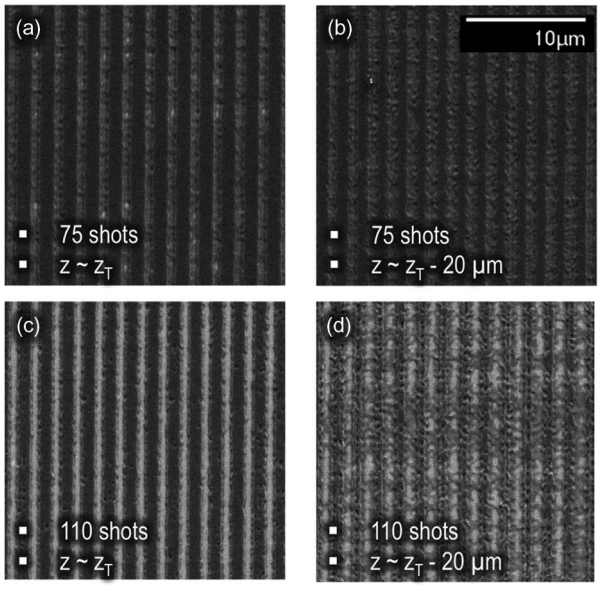

Fig. 5. Patterned photoresist images by self-imaging technique. The exposure dose and the distance cause the different qualities in the result.

where the A is the area of the mask [4]. With the experimental parameters used the DOF is ~600 nm for the first Talbot plane, $n = 1$.

The print was recorded on a silicon wafer spin-coated with 50 nm thick layer of photoresist (JSR Inc.). During the exposure, the distance from the wafer to mask was maintained close to the first Talbot distance. After the exposure, the exposed photoresist was developed for 30 seconds and rinsed with 2-Propanol. Fig. 5 shows SEM images of the patterned photoresist. The quality of the grid pattern is improved when the wafer is close to $z = z_T$ (a), (c), rather than

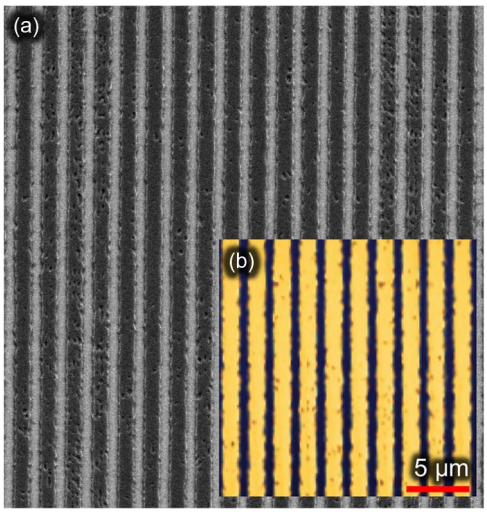

Fig. 6. Patterned photoresist measured with SEM and AFM (right bottom image).

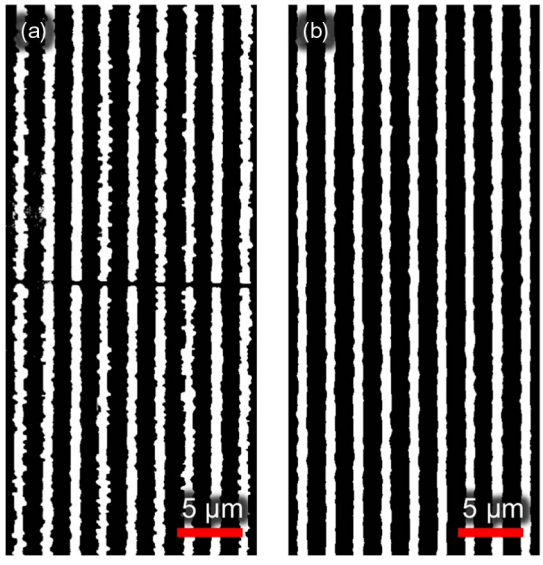

Fig. 7. (a) Mask image and (b) self-image after the binary image conversion.

in the case when the wafer is out of focus (b), (d). The quality improvement is significant when the distance is precisely controlled to be the Talbot distance. The quality also depends on the exposure time, because the threshold of intensity impacts the development results, as shown in Fig. 5(a), (c) and (b), (d) that the photoresists were exposed with 75 and 110 shots, respectively. Fig. 6(a) is the zoomed-in image of Fig. 5(c). Fig. 6(b) is an AFM image taken at the central part of sample. The roughness is significantly decreased in the print as compared to the roughness in the mask.

4. Results and Discussions

In order to compare the roughness in the mask and the one in the self-image, the images shown in Figs. 4 and 6(b) were converted into binary images as shown in Fig. 7. In this case, the gray-scale image turns into the binary image by the balanced histogram thresholding method (BHT).

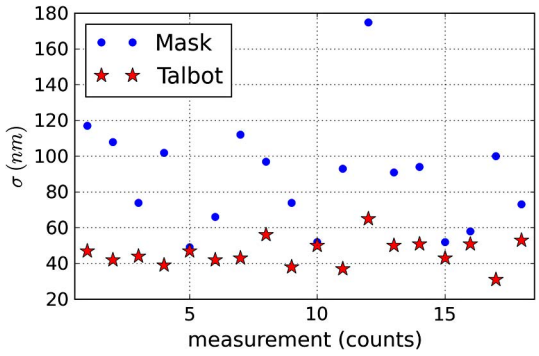

Fig. 8. The σ values in the mask and Talbot patterns.

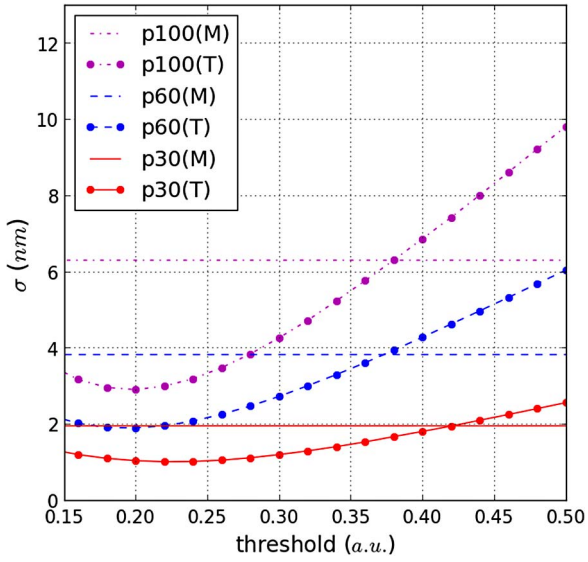

Fig. 9. Simulation result: σ curves in masks (*M*) and in self-images (*T*) for the pitches of 100, 60, and 30 nm.

The pixels fall within a desired range of intensity value, thus the image is divided to black or white from two main classes: background and foreground [19]. The improvement of quality can be seen in Fig. 7(a) and (b). This apparent improvement correlates well with the reduction of the σ. Fig. 8 plots the calculated σ for the mask and the Talbot image for 18 locations along the edges of the slits. The σ measured in the print are significantly lower than those in mask. The average values are $\sigma = 88$ nm in mask and $\sigma = 46$ nm in the print. The σ measured in the experimental result correlates well with the σ obtained in the simulation assuming a threshold for the binarization in the range 0.15–0.3 in Fig. 3. In both simulation and experiment, the σ values are reduced by about a factor of 2 or more.

We also analyzed the influence of the pitch, the slit width and the σ of the mask to the quality of the print. The study has completed by measuring the roughness of the Talbot image obtained with different masks.

First, to evaluate the influence of the pitch, we tested three different masks. The mask pitches were $p = 100$ nm, $p = 60$ nm, $p = 30$ nm. In those pitches, the roughness was $\sigma = 6.2$ nm, $\sigma = 3.9$ nm, and $\sigma = 2$ nm respectively. Due to the averaging characteristic of the Talbot effect, the σ in the self-image became $\sigma > 3$ nm, $\sigma > 2$ nm, and $\sigma > 1$ nm respectively. The σ in the mask (*M*) and at the Talbot plane (*T*) for selected pitches are plotted in Fig. 9.

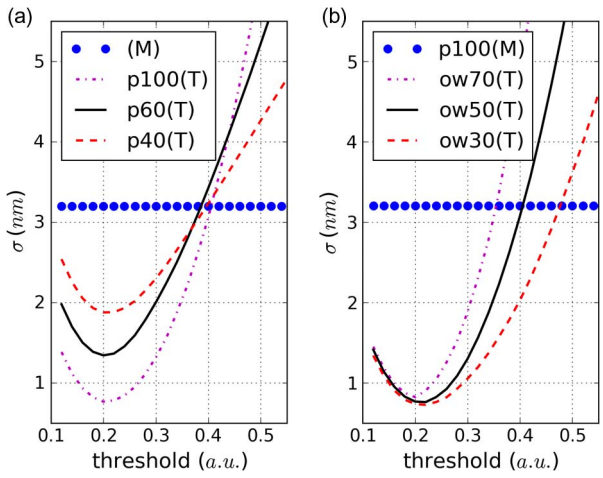

Fig. 10. Simulation results for various parameters. (a) The σ at z_T (T) for pitches of 100, 60, and 40 nm when an identical σ (M) in mask is used. (b) The σ at z_T (T) for opening widths of 100, 70, and 50 nm when a fixed 100-nm pitch and $\sigma = 3.2$ nm in the mask are used.

The complete lithography method includes processes that determine the quality of the print. The printed result is influenced by the photoresist response and the development process among other factors. However, the analysis presented here with the thresholding method in the areal image is intended to study only the self-healing effect in the optical image. As discussed in Fig. 3, when we assume a threshold around 0.3 the simulation and the experimental results are in good agreement. Using this value for the threshold, the parameter σ in the self-image becomes 4 nm, 2.1 nm and 1.1 nm, respectively. This represents a significant improvement of the self-imaging for sub-100 nm pitch gratings. The roughness is reduced by ~50% for all three masks with different pitches and initial values of the sigma. This amount of improvement is expected for all pitches considered in this analysis.

Second, we tested various mask pitches with identical σ. From this simulation, we used EUV illumination at 13.5 nm wavelength, which is a candidate for the source of the next generation of optical lithography. The pitches selected for this test were 100 nm, 60 nm and 40 nm, with σ in the three cases fixed at 3.2 nm in mask. As shown in Fig. 10(a), the σ in the self-image is decreased from ~2 nm to ~1 nm as the pitch is increased from 40 nm to 100 nm. Our analysis indicates that the resulting sigma in the Talbot image is proportional to the ratio of the initial sigma and the slit-width (pitch/2) in the mask. Therefore, in Fig. 10(a), the sigma for the mask with high-dense grid is increased in comparison to the one for the mask with low-dense grid.

Lastly, the slit-width was varied with fixed pitch and σ in the mask. The values of the slit-width were 70 nm, 50 nm, and 30 nm, where a fixed pitch of 100 nm and a fixed $\sigma = 3.2$ nm in the mask. As can be seen in Fig. 10(b), the minimum σ values in the self-image were ~0.9 nm. However the dependence on thresholding is different in the three cases enabling wider threshold values for smaller slit widths. For example, for $\sigma = 2$ nm, the threshold increases as the slit width (ow) is decreased as shown in Fig. 10(b). This implies that the fabrication requirements can be relaxed with adjustment of the slit-width. Those results can be of a great interest in nano-patterning, where the line-edge roughness (LER) is one of the significant issues in electronic device fabrication.

5. Conclusion

In conclusion, we have demonstrated a submicron printing technique based on self-imaging and performed a detailed characterization of the quality improvement in the print relative to the mask. The rough grid pattern on the mask produces a self-image with line-edge roughness reduced by about a factor of 2 for 2 μm to 30 nm pitch gratings. This is due to the fact that line

edges are randomly rough in the mask, which forms a smeared self-image that averages the roughness effectively reducing the σ. The improvement in the Talbot image is determined by the number of diffraction orders involved which in turn depends on the particular configuration (numerical aperture and periodicity) of the mask [20]. In the simulation, the σ is improved in self-images for sub 30 nm pitch when EUV radiation is assumed in the illumination.

Acknowledgment

The authors would like to thank E. Neumann at the Helmholtz Nanoelectronic Facility, Forschungszentrum Juelich, for help with FIB milling.

References

[1] D. Gruetzmacher *et al.*, "Three-dimensional Si/Ge quantum dot crystals," *Nano Lett.*, vol. 7, no. 10, pp. 3150–3156, 2007.
[2] H. F. Talbot, "LXXXVI. Facts relating to optical science no. IV," *Philos. Mag.*, vol. 9, no. 56, pp. 401–407, Dec. 1836.
[3] L. Rayleigh, "XXV. On diffraction-gratings, and on some phenomena connected therewith," *Philos. Mag.*, vol. 11, no. 67, pp. 196–205, Dec. 1881.
[4] A. Isoyan *et al.*, "Talbot lithography: Self-imaging of complex structures," *J. Vac. Sci. Technol. B, Microelectron. Nanometer Struct.*, vol. 27, no. 6, pp. 2931–2937, Dec. 2009.
[5] H. H. Solak and Y. Ekinci, "Achromatic spatial frequency multiplication: A method for production of nanometer-scale periodic structures," *J. Vac. Sci. Technol. B*, vol. 23, no. 6, pp. 2705–2710, Dec. 2005.
[6] L. Urbanski *et al.*, "Defect-tolerant extreme ultraviolet nanoscale printing," *Opt. Lett.*, vol. 37, no. 17, pp. 3633–3635, Sep. 2012.
[7] H. Dammann, G. Groh, and M. Kock, "Restoration of faulty images of periodic objects by means of self-imaging," *Appl. Opt.*, vol. 10, no. 6, pp. 1454–1455, Jun. 1971.
[8] A. Lohmann and J. Thomas, "Making an array illuminator based on the Talbot effect," *Appl. Opt.*, vol. 29, no. 29, pp. 4337–4340, Oct. 1990.
[9] T. Sato *et al.*, "Printability of defects in Talbot lithography," *Microelectron. Eng.*, vol. 143, pp. 21–24, Mar. 2015.
[10] M. Hofmann, R. Kampmann, and S. Sinzinger, "Perturbed Talbot patterns for the measurement of low particle concentrations in fluids," *Appl. Opt.*, vol. 51, no. 10, pp. 1605–1615, Apr. 2012.
[11] G. Druart *et al.*, "Nonparaxial analysis of continuous self-imaging gratings in oblique illumination," *J. Opt. Soc. Amer. A, Opt. Image Sci. Vis.*, vol. 24, no. 10, pp. 3379–3387, Oct. 2007.
[12] W. Li *et al.*, "Defect-free periodic structures using extreme ultraviolet Talbot lithography in a tabletop system," *J. Vac. Sci. Technol. B*, vol. 31, no. 6, pp. 1–7, Nov./Dec. 2013.
[13] J. W. Goodman, *Introduction to Fourier Optics*, 2nd ed. New York, NY, USA: McGraw-Hill, 1996.
[14] C. Macchietto, B. R. Benware, and J. J. Rocca, "Generation of millijoule-level soft-X-ray laser pulses at a 4-Hz repetition rate in a highly saturated tabletop capillary discharge amplifier," *Opt. Lett.*, vol. 24, no. 16, pp. 1115–1117, Aug. 1999.
[15] Y. Liu *et al.*, "Achievement of essentially full spatial coherence in a high-average-power soft-X-ray laser," *Phys. Rev. A*, vol. 63, no. 3, pp. 1–5, Feb. 2001.
[16] M. C. Marconi, J. L. A. Chilla, C. H. Moreno, B. R. Benware, and J. J. Rocca, "Measurement of the spatial coherence buildup in a discharge pumped table-top soft X-ray laser," *Phys. Rev. Lett.*, vol. 79, no. 15, pp. 2799–2802, Oct. 1997.
[17] L. Urbanski *et al.*, "Spectral linewidth of a Ne-like Ar capillary discharge soft-X-ray laser and its dependence on amplification beyond gain saturation," *Phys. Rev. A*, vol. 85, no. 3, pp. 1–5, Mar. 2012.
[18] H. Kim *et al.*, "Fractional Talbot lithography with extreme ultraviolet light," *Opt. Lett.*, vol. 39, no. 24, pp. 6969–6972, Dec. 2014.
[19] A. Anjos and H. Shahbazkia, "Bi-level image thresholding—A fast method," *Biosignals*, vol. 2, pp. 70–76, Jan. 2008.
[20] M. Kim, T. Scharf, C. Menzel, C. Rockstuhl, and H. Herzig, "Talbot images of wavelength-scale amplitude gratings," *Opt. Exp.*, vol. 20, no. 5, pp. 4903–4920, Feb. 2012.